Ground-state chiral excitation via periodic modulation

Shuyue Wang,[1] Wuji Zhang,[1] Chunfang Sun,[1] Chunfeng Wu,[2] and Gangcheng Wang[1,3,*]

[1]*Center for Quantum Sciences and School of Physics, Northeast Normal University, Changchun 130024, China*

[2]*Science, Mathematics and Technology, Singapore University of Technology and Design, 8 Somapah Road, Singapore 487372, Singapore*

[3]*Key Laboratory of Advanced Optical Manufacturing Technologies of Jiangsu Province, Soochow University, Suzhou 215006, China*

(Received 18 March 2024; accepted 20 June 2024; published 10 July 2024)

In this study we engineer the z component of the Dzyaloshinskii-Moriya interaction mediated by photons to emulate ground-state chiral excitation based on three-level atoms driven by quantum and classical fields. We employ adiabatic elimination techniques to derive an effective Dzyaloshinskii-Moriya interaction Hamiltonian of two-level systems in the ground-state manifold, which can ensure the desired dynamics is achieved through the implementation of periodic modulation. Meanwhile, three-state and multistate chiral excitation can be obtained by choosing appropriate driving frequencies and phases. The numerical simulation results clearly indicate that our proposal can generate the comparatively perfect three-state chiral excitation and relatively reliable multistate chiral excitation. Moreover, the influence of unfavorable factors on the chiral current is discussed in detail, and the potential experimental feasibility further shows that our results provide possibilities for quantum state transfer and future quantum networks.

DOI: 10.1103/PhysRevA.110.012432

I. INTRODUCTION

Photon-mediated excitation exchange [1–3], as a well-established paradigm in quantum simulations, has garnered significant attention due to its pivotal role in testing the fundamentals of quantum mechanics [4,5]. In particular, spin-exchange interactions mediated by vacuum fields within cavities have been investigated from solely scientific discovery to the foundational engineering associated with the design of multiqubit quantum systems [6–8]. Overall, the optical manipulation of analogous interactions involves two-photon coupling between energy levels including hyperfine and Zeeman states. Such an approach allows for the encoding of spin states in long-lived ground states, which can enable the generation of remarkable coherent characteristics and a robust exchangeable scheme [9–13]. In addition, this encoding provides an intriguing possibility for further exploration of higher spin models [14–16] and the preparation of squeezed-state quantum metrology [17,18].

The Dzyaloshinskii-Moriya interaction (DMI) [19,20], originating from relativistic antisymmetric exchange interactions, can induce a range of chiral phenomena, such as spin spirals and skyrmions [21,22], which have been harnessed in spintronics to engineer spin structures with topological chiral conservation. Recently, the DMI has been simulated based on Floquet engineering [23], which offers a route for exploring quantum spin chirality. Meanwhile, spin chirality originating from antisymmetric spin-exchange interactions has been experimentally verified in a superconducting qubit platform [24]. Unlike spin chiral operators [25], the z component of the DMI breaks parity symmetry (exchanging $\vec{\sigma}_j$ with $\vec{\sigma}_k$) while preserving time-reversal symmetry (replacing $\vec{\sigma}_j$ by $-\vec{\sigma}_j$). This property enables the realization of both the chiral spin current and two opposing directions of spin-excited chiral evolution while reversing the initial states of all spins [24]. It is worth mentioning that the phenomenon is similar to the quantum spin Hall effect [26–29], where electrons traveling in opposite directions along the edges of a material possess opposing spins. Up to now, spin chirality [30] has been successfully implemented on various platforms, such as hybrid cavity-magnon systems [31], synthetic magnetic fields [32], superconducting circuits [33], Rydberg atoms [34–36], circuit QED [37–39], and ion clusters [40]. Due to its favorable properties, it holds promise in the preparation of entangled states [24], the quantum Hall effect [41], chiral spin liquids [42,43], quantum state transfer [44], chiral separation [45], and stabilization of skyrmions [46,47]. Nevertheless, these previous studies have demonstrated perfect chiral current in a triangular three-node network and failed to work in larger networks. The existence of flawless chiral current in multinode networks remains an open question, which is crucial for advancing applications in lattices with nontriangular structure.

In parallel, periodic modulation [48–52] stands as a pivotal technique across signal processing, communications, and control systems, characterized by the transmission of information through systematic alterations in specific signal parameters. This methodology encompasses a spectrum of techniques such as amplitude modulation [53], frequency modulation [54], and phase modulation [55], among others. These approaches significantly enhance the controllability of quantum systems and pave the way for the development of more robust schemes. An intriguing question arises: Can the incorporation of periodic modulation into ground-state chiral current yield analogous beneficial outcomes? This question motivates us to delve into the exploration of chiral current through periodic modulation.

*Contact author: wanggc887@nenu.edu.cn

In this paper we propose a theoretical scheme for realizing the DMI within the hyperfine ground-state manifold of three-level atoms by applying periodic modulation, which gives rise to the generation of chiral current in three-level atomic chains. Specifically, the effective Hamiltonian can be derived by employing the technique of adiabatic elimination and perturbative expansion. Furthermore, we investigate how to generate three- and multistate chiral currents within various Dzyaloshinskii-Moriya-type interactions. The description of numerical simulation results reveals that our scheme can achieve extremely reliable chiral current in the ground state. Additionally, we give a thorough explanation of the effective conditions of the model and experimental scheme.

The remainder of this paper is organized as follows. In Sec. II we present a detailed process for the derivation of the effective Hamiltonian and discuss the dynamics of three- and multistate chiral currents by adjusting the phase and driving frequencies. In Sec. III the effective master equation involving only the ground-state manifold is obtained by combining the theory of the density operator and adiabatic elimination of the excited states, and the simulation results show that our scheme can generate the desired ground-state chiral current. Furthermore, we provide a detailed explanation for the effective conditions of the model and its experimental operability. We give a comprehensive summary of the entire paper and provide an outlook for chiral current research in Sec. IV.

II. EFFECTIVE DMI AND CHIRALITY

A. Derivation of the effective Hamiltonian

We consider the simulation of the DMI and chiral current by trapping cold atoms in an intracavity lattice [56–58]. In our proposed scheme, the common single-mode cavity mediates the interactions between atoms at different lattice sites. In Fig. 1 we adopt a three-level system in a Λ configuration, consisting of two lower-energy states $|s\rangle$ and $|g\rangle$, along with an excited state $|e\rangle$. The pump beam and the cavity mode separately couple two legs of the configuration while applying the periodic driving field at the atomic ground-state transition frequency. The Hamiltonian is initially written under the rotating wave approximation as (hereafter we set $\hbar = 1$)

$$\hat{H}(t) = \hat{H}_C + \hat{H}_A(t) + \hat{H}_{LM} + \hat{H}_P(t), \tag{1}$$

where

$$\hat{H}_C = \omega_c \hat{a}^\dagger \hat{a}, \tag{2a}$$

$$\hat{H}_A(t) = \sum_k \omega_e \hat{\sigma}_k^{ee} + \omega_k^g(t)\hat{\sigma}_k^{gg}, \tag{2b}$$

$$\hat{H}_{LM} = \sum_k g\hat{a}\hat{\sigma}_k^{eg} + \text{H.c.}, \tag{2c}$$

$$\hat{H}_P(t) = \sum_k \frac{\Omega_k}{2}\hat{\sigma}_k^{se} e^{i\omega_k^L t} + \text{H.c.} \tag{2d}$$

The denotation $\hat{a}$ ($\hat{a}^\dagger$) is the annihilation (creation) operator of the cavity field with frequency ω_c. The denotation ω_e represents the assisted excited state $|e\rangle$ of the atomic energy and the two internal atomic states $\{|s\rangle, |g\rangle\}$ in the hyperfine manifold denote the pseudospin-$\frac{1}{2}$ state with the energy-level splitting $\omega_k^g(t)$, where $\hat{\sigma}_k^{ab} = |a\rangle_k\langle b|$ corresponds to three

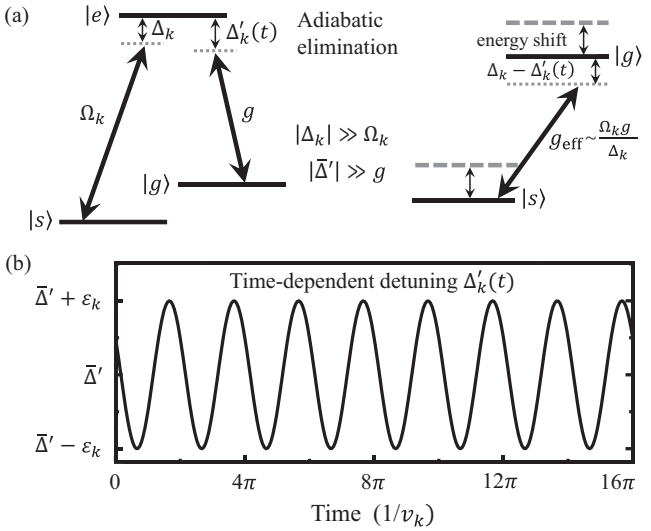

FIG. 1. (a) Schematic diagram of the Λ-type three-level atom. Here $\{|s\rangle, |g\rangle, |e\rangle\}$ depicts three atomic energy levels with energies $\{0, \omega_g, \omega_e\}$, respectively. The pump laser with Rabi frequency Ω_k and frequency ω_k^L induces a σ transition between atomic ground $|s\rangle$ and excited state $|e\rangle$. A photon mode with coupling strength g and frequency ω_c induces a π transition between $|g\rangle$ and $|e\rangle$. Under the condition of large detuning i.e., $|\Delta_k| \gg \Omega_k$ and $|\bar{\Delta}'| \gg g$, the transitions between the two ground states $|s\rangle$ and $|g\rangle$ with the effective coupling strength $g_{\text{eff}} \sim \Omega_k g/\Delta_k$ and the effective detuning $\Delta_k - \Delta_k'(t)$ can be mediated by adiabatic elimination. (b) Time-dependent detuning $\Delta_k'(t)$ as a function of evolution time t. Here $\bar{\Delta}' \pm \varepsilon_k$ represent the maximum and minimum detuning, with $\bar{\Delta}'$ the average detuning.

atomic energy levels $a, b = \{s, g, e\}$ and k marks the position. The time-dependent frequency takes the form $\omega_k^g(t) = \omega_g + \varepsilon_k \cos(\nu_k t - \phi_k)$, with the amplitude ε_k, frequency ν_k, and phase ϕ_k acting on the kth atom [59–62]. Such a frequency-modulated term can be induced by a time-dependent Stark shift [63,64]. The g denotes the coupling strength between atoms and the cavity. The transition between $|s\rangle$ and $|e\rangle$ is driven by an external local pump field with frequency ω_k^L and Rabi frequency Ω_k. Moving to the rotation frame defined by $\hat{U}(t) = \exp[-i\sum_k(\omega_k^L\hat{\sigma}_k^{ee} + \omega_g\hat{\sigma}_k^{gg})t]e^{-i\omega_c\hat{a}^\dagger\hat{a}t}$, the transformed Hamiltonian can be expressed as

$$\begin{aligned}\hat{\tilde{H}}(t) &= \hat{U}^\dagger(t)[\hat{H}(t) - i\partial_t]\hat{U}(t) \\ &= \hat{\tilde{H}}_A(t) + \hat{\tilde{H}}_{LM}(t) + \hat{\tilde{H}}_P,\end{aligned} \tag{3}$$

where

$$\hat{\tilde{H}}_A(t) = \sum_k \Delta_k\hat{\sigma}_k^{ee} + \varepsilon_k\cos(\nu_k t - \phi_k)\hat{\sigma}_k^{gg}, \tag{4a}$$

$$\hat{\tilde{H}}_{LM}(t) = \sum_k g\hat{a}\hat{\sigma}_k^{eg} e^{i(\bar{\Delta}' - \Delta_k)t} + \text{H.c.}, \tag{4b}$$

$$\hat{\tilde{H}}_P = \sum_k \frac{\Omega_k}{2}\hat{\sigma}_k^{se} + \text{H.c.} \tag{4c}$$

Here $\Delta_k = \omega_e - \omega_k^L$ and $\bar{\Delta}' = \omega_e - \omega_g - \omega_c$, with $\Delta_k'(t) = \omega_e - \omega_k^g(t) - \omega_c$. In the large-detuning framework, the frequencies of both the cavity mode and Raman fields are far

detuned to the atomic transition, i.e., $|\Delta_k| \gg \Omega_k$ and $|\bar{\Delta}'| \gg g$. Assuming a Λ-type system characterized by a significant detuning between atoms and driving fields, the technique of adiabatic elimination [65–67] can be employed to derive an effective Hamiltonian. For the system considered in this work, we can introduce two orthogonal projection operators $\hat{P} = \sum_k(\hat{\sigma}_k^{gg} + \hat{\sigma}_k^{ss})$ and $\hat{Q} = \sum_k \hat{\sigma}_k^{ee}$. The effective Hamiltonian can be recast as

$$\begin{aligned}\hat{H}'(t) &= \hat{P}\hat{\tilde{H}}(t)\hat{P} - \hat{P}\hat{\tilde{H}}(t)\hat{Q}\frac{1}{\hat{Q}\hat{\tilde{H}}(t)\hat{Q}}\hat{Q}\hat{\tilde{H}}(t)\hat{P} \\ &= \hat{H}'_0(t) + \hat{H}'_{\rm int}(t), \end{aligned} \tag{5}$$

where

$$\hat{H}'_0(t) = \sum_k \left(\omega_k^g(t) - \omega_g - \frac{g^2}{\Delta_k}\hat{a}^\dagger\hat{a}\right)\hat{\sigma}_k^{gg} - \sum_k \frac{\Omega_k^2}{4\Delta_k}\hat{\sigma}_k^{ss}, \tag{6a}$$

$$\hat{H}'_{\rm int}(t) = -\sum_k \left(\frac{\Omega_k g}{2\Delta_k}\hat{a}^\dagger\hat{\sigma}_k^{gs}e^{-i(\bar{\Delta}'-\Delta_k)t} + \text{H.c.}\right). \tag{6b}$$

Following the adiabatic elimination of the excited state, each atom can be considered as a gg-type qubit. Due to the large detuning in frequency between the photon mode and the atom, it is obvious that the excitation process cannot be achieved through photon-atom interaction and the mode a will not be excited [68]. Therefore, the term $\sum_k(g^2/\Delta_k)\hat{a}^\dagger\hat{a}\hat{\sigma}_k^{gg}$, which scales with the average photon number, can be safely neglected.

For the sake of facilitating the discussion, the Hamiltonian is converted into the interaction picture with respect to the time-dependent unitary operator

$$\begin{aligned}\hat{U}_0(t) &= \exp\left(-i\int_0^t dt'\hat{H}'_0(t')\right) \\ &= \exp\left[-i\sum_k\left(\frac{\varepsilon}{\nu}\sin(\nu t - \phi_k) + \beta_k\right)\hat{\sigma}_k^{gg}\right. \\ &\quad \left. + i\sum_k \frac{\Omega_k^2}{4\Delta_k}\hat{\sigma}_k^{ss}t\right], \end{aligned} \tag{7}$$

where $\beta_k = (\varepsilon/\nu)\sin\phi_k$. For convenience, we assume here a uniform amplitude $\varepsilon_k = \varepsilon$ and frequency $\nu_k = \nu$. We obtain the interaction between photons and qubits with $\delta_k = \bar{\Delta}' - \Delta_k - \Omega_k^2/4\Delta_k$ and the transformed Hamiltonian

$$\begin{aligned}\hat{H}_I(t) = \hat{U}_0^\dagger(t)[\hat{H}'(t) - i\partial_t]\hat{U}_0(t) &= -\sum_k \frac{\Omega_k g}{2\Delta_k}\hat{a}\hat{\sigma}_k^{sg} \\ &\times \exp\left\{i\left[\delta_k t - \left(\frac{\varepsilon}{\nu}\sin(\nu t - \phi_k) + \beta_k\right)\right]\right\} + \text{H.c.} \end{aligned} \tag{8}$$

It is worth mentioning that the site-dependent phase factor β_k can be gauged away from the Hamiltonian by performing the unitary transformation $\hat{R} = \prod_{k=1}^N e^{i\beta_k\hat{\sigma}_k^z/2}$ on the Hamiltonian in Eq. (8). Then we can tune ω_k^L so that $\delta_k = 0$, i.e., $\bar{\Delta}' = \Delta_k + \Omega_k^2/4\Delta_k$. Using the Jacobi-Anger identity $e^{iz\sin\theta} = \sum_{n=-\infty}^{\infty}\mathcal{J}_n(z)e^{in\theta}$, where $\mathcal{J}_n(z)$ represents the nth-order Bessel function of the first kind, the Hamiltonian in Eq. (8) can be rewritten as

$$\hat{H}_I(t) = -\sum_k\sum_{n=-\infty}^{\infty}\frac{\Omega_k g}{2\Delta_k}\mathcal{J}_n\left(-\frac{\varepsilon}{\nu}\right)e^{in(\nu t-\phi_k)}\hat{a}\hat{\sigma}_k^{sg} + \text{H.c.} \tag{9}$$

The above Hamiltonian can be rewritten in the Fourier form

$$\hat{H}_I(t) = \sum_{n=-\infty}^{\infty}\hat{H}_n e^{in\nu t},$$

where

$$\hat{H}_n = -\sum_k \frac{\Omega_k g}{2\Delta_k}\mathcal{J}_n\left(\frac{\varepsilon}{\nu}\right)e^{-in\phi_k}\left[(-1)^n\hat{a}\hat{\sigma}_k^{sg} + \hat{a}^\dagger\hat{\sigma}_k^{gs}\right]. \tag{10}$$

We consider the condition where the external driving frequency is significantly high and far exceeds the characteristic energy inside the system, i.e., $\nu \gg \Omega_k g/|\Delta_k|$. As a result, introducing the Pauli operators $\hat{\sigma}_k^x = \hat{\sigma}_k^{gs} + \hat{\sigma}_k^{sg}$ and $\hat{\sigma}_k^y = i(\hat{\sigma}_k^{sg} - \hat{\sigma}_k^{gs})$, we can employ perturbative expansion techniques [48] to derive an approximate effective Hamiltonian by truncating to powers of $1/\nu$ as

$$\begin{aligned}\hat{H}_{\rm eff} &= \hat{H}_0 + \sum_{n=1}^{\infty}\frac{1}{n\nu}[\hat{H}_n, \hat{H}_{-n}] \\ &= -\sum_k \frac{\Omega_k g}{2\Delta_k}\mathcal{J}_0\left(\frac{\varepsilon}{\nu}\right)\left(\hat{a}\hat{\sigma}_k^{sg} + \hat{a}^\dagger\hat{\sigma}_k^{gs}\right) \\ &\quad + \sum_{k>l}\sum_{n=1}^{\infty}\frac{\Omega_l\Omega_k g^2}{4n\nu\Delta_l\Delta_k}\mathcal{J}_n^2\left(\frac{\varepsilon}{\nu}\right)\sin(n\phi_{lk})\left(\hat{\sigma}_l^x\hat{\sigma}_k^y - \hat{\sigma}_l^y\hat{\sigma}_k^x\right), \end{aligned} \tag{11}$$

where $\hat{H}_{-n}$ and $\hat{H}_n$ satisfy the relation $\hat{H}_{-n} = \hat{H}_n^*$ and $\phi_{lk} = \phi_l - \phi_k$. Third-order and even higher-order terms are analyzable using the James effective Hamiltonian method [69]. For the dispersion region of concern in this study, these terms have minimal impact on the results and can be safely omitted. By adjusting the appropriate ratio of the driving intensity ε and frequency ν, specifically setting $\varepsilon/\nu = 2.4048$, the first term vanishes and the effective Hamiltonian in Eq. (11) can be recast in the form

$$\hat{H}_{\rm eff} = \sum_{k>l}\sum_{n=1}^{\infty}\frac{\Omega_l\Omega_k g^2}{4n\nu\Delta_l\Delta_k}\mathcal{J}_n^2\left(\frac{\varepsilon}{\nu}\right)\sin(n\phi_{lk})\left(\hat{\sigma}_l^x\hat{\sigma}_k^y - \hat{\sigma}_l^y\hat{\sigma}_k^x\right). \tag{12}$$

Thus, we obtain an effective tunable DMI Hamiltonian with a z component. In contrast, recent studies have utilized Floquet engineering to design the pulse sequence [70–74], which could give rise to the simulation of the complete DMI as much as possible under the more accurate multiorder Trotter-Suzuki expansion [75,76]. This approach can enable us to perform operations that are unattainable through conventional methods, thereby enhancing the efficiency and reliability of quantum computing and quantum information processing. In short, such a complex process effectively allows us to derive two other components of the DMI by introducing the obtained z component and thus realize the desired chiral dynamics [77].

B. Three-state chiral current

With controllable parameters to implement the desired dynamics, we now present some examples of three-state chiral current.

1. Three-atom case

We first begin by examining the scenario for $N = 3$ atoms, as this case is crucial for comprehending the chiral dynamics within the system under consideration. We perform the dynamical analysis by choosing proper site-dependent phases with $\phi_k = 2k\pi/3$ $(k = 1, 2, 3)$. The effective Hamiltonian containing the z component of the DMI can be obtained as

$$\hat{H}_{\text{eff}}^{(3)} = -\kappa \sum_{k=1}^{3} \left(\hat{\sigma}_k^x \hat{\sigma}_{k+1}^y - \hat{\sigma}_k^y \hat{\sigma}_{k+1}^x\right). \tag{13}$$

Note that if $k = 3$, then $k + 1 \equiv 1$, and the effective coupling strength is

$$\kappa = \frac{\Omega^2 g^2}{4\Delta^2 \nu} \sum_{n=1}^{\infty} \mathcal{J}_n^2\left(\frac{\varepsilon}{\nu}\right) \sin\left(\frac{2n\pi}{3}\right) \Big/ n, \tag{14}$$

where $\Omega_k = \Omega$, $\omega_k^L = \omega_L$, and $\Delta_k = \Delta$. Then we can represent the above effective Hamiltonian in its ground-state subspace spanned by $\{|gss\rangle, |sgs\rangle, |ssg\rangle\}$ as

$$\hat{H}_{\text{sub}}^{(3)} = 2i\kappa \begin{pmatrix} 0 & -1 & 1 \\ 1 & 0 & -1 \\ -1 & 1 & 0 \end{pmatrix}. \tag{15}$$

The eigenvalues for $\hat{H}_{\text{sub}}^{(3)}$ are $\{0, \pm\omega\}$ with $\omega = 2\sqrt{3}\kappa$. Therefore, the corresponding time-evolution operator can be written as

$$\hat{U}(t) = \begin{pmatrix} x_1(t) & x_3(t) & x_2(t) \\ x_2(t) & x_1(t) & x_3(t) \\ x_3(t) & x_2(t) & x_1(t) \end{pmatrix}, \tag{16}$$

where

$$\begin{aligned} x_1(t) &= \tfrac{1}{3}[1 + 2\cos(\omega t)], \\ x_2(t) &= \tfrac{1}{3}\left[1 + 2\cos\left(\omega t - \tfrac{2}{3}\pi\right)\right], \\ x_3(t) &= \tfrac{1}{3}\left[1 + 2\cos\left(\omega t - \tfrac{4}{3}\pi\right)\right]. \end{aligned} \tag{17}$$

Initialing the initial state as $|\psi(0)\rangle = |gss\rangle$ and acting the evolution operator $\hat{U}(t)$ on the initial state, we can obtain the time-evolution state

$$|\psi(t)\rangle = x_1(t)|gss\rangle + x_2(t)|sgs\rangle + x_3(t)|ssg\rangle. \tag{18}$$

It can be easily verified that

$$|\psi(t)\rangle = \begin{cases} |gss\rangle, & t = 2n\pi/2\sqrt{3}\kappa \\ |sgs\rangle, & t = (2\pi/3 + 2n\pi)/2\sqrt{3}\kappa \\ |ssg\rangle, & t = (4\pi/3 + 2n\pi)/2\sqrt{3}\kappa. \end{cases} \tag{19}$$

Here n is an integer. Thus the state $|g\rangle$ traverses the ring sites in a counterclockwise manner, i.e., $1 \to 2 \to 3 \to 1 \to \cdots$.

Similarly, the time-evolution operator in the corresponding ground-state subspace spanned by $\{|sgg\rangle, |gsg\rangle, |ggs\rangle\}$ can be represented as $\hat{U}^\dagger(t)$. If we set the initial state as $|\psi(0)\rangle = |sgg\rangle$, the evolution state is

$$|\psi(t)\rangle = x_1(t)|sgg\rangle + x_3(t)|gsg\rangle + x_2(t)|ggs\rangle.$$

We can obtain

$$|\psi(t)\rangle = \begin{cases} |sgg\rangle, & t = 2n\pi/2\sqrt{3}\kappa \\ |ggs\rangle, & t = (2\pi/3 + 2n\pi)/2\sqrt{3}\kappa \\ |gsg\rangle, & t = (4\pi/3 + 2n\pi)/2\sqrt{3}\kappa. \end{cases} \tag{20}$$

The state $|s\rangle$ traverses the ring sites in a clockwise manner, i.e., $1 \to 3 \to 2 \to 1 \to \cdots$.

For the case of more than three atoms, three-state chiral current can be investigated by introducing composite spins. Compared with Ref. [24], we can tune the Rabi frequencies and the phases to obtain perfect chiral current.

2. Four-atom case

For the case of four atoms, the second and third effective spins can be grouped as a composite spin with $s = 1$. Here we choose the initial conditions $\phi_1 = 2\pi/3, \phi_2 = \phi_3 = 4\pi/3$, $\phi_4 = 2\pi$, $\Omega_1 = \Omega_4 = \Omega$, and $\Omega_2 = \Omega_3 = \Omega/\sqrt{2}$. The corresponding effective Hamiltonian can be written as

$$\hat{H}_{\text{eff}}^{(4)} = -\kappa \vec{e}_z \cdot \left(\frac{1}{\sqrt{2}}\vec{\sigma}_1 \times \vec{\Sigma}_{23} + \vec{\sigma}_4 \times \vec{\sigma}_1 + \frac{1}{\sqrt{2}}\vec{\Sigma}_{23} \times \vec{\sigma}_4\right), \tag{21}$$

where the composite operator $\vec{\Sigma}_{23} = \vec{\sigma}_2 + \vec{\sigma}_3$ with spin 1. Here we can consider Δ_k to be approximately equal to Δ. In this situation, we adopt the triplet form to describe the chiral evolution concisely, and the quantum states can be expressed as

$$|\mathcal{T}_-\rangle = |ss\rangle, \quad |\mathcal{T}_0\rangle = \frac{1}{\sqrt{2}}(|gs\rangle + |sg\rangle), \quad |\mathcal{T}_+\rangle = |gg\rangle.$$

The representation of the Hamiltonian in Eq. (21) in the ground-state subspace spanned by $\{|g\mathcal{T}_- s\rangle, |s\mathcal{T}_0 s\rangle, |s\mathcal{T}_- g\rangle\}$ is identical to that in Eq. (15). Similarly, within the ground-state subspace spanned by $\{|s\mathcal{T}_+ g\rangle, |g\mathcal{T}_0 g\rangle, |g\mathcal{T}_+ s\rangle\}$, the time-evolution operator can also be denoted by $\hat{U}^\dagger(t)$.

3. Five-atom case

For the case of five atoms, we set three different modulation phases. The first type of phase distribution can modulate the interaction between a site with spin $\frac{1}{2}$ and two composite sites with spin 1. The phases are set to be $\phi_1 = 2\pi/3$, $\phi_2 = \phi_3 = 4\pi/3$, $\phi_4 = \phi_5 = 2\pi$, $\Omega_1 = \Omega$, and $\Omega_k = \Omega/\sqrt{2}$ with $k = 2, 3, 4, 5$. The system evolution is governed by the effective Hamiltonian

$$\begin{aligned} &\hat{H}_{\text{eff}}^{(5,1)} \\ &= -\kappa \vec{e}_z \cdot \left(\frac{1}{\sqrt{2}}\vec{\sigma}_1 \times \vec{\Sigma}_{23} + \frac{1}{\sqrt{2}}\vec{\Sigma}_{45} \times \vec{\sigma}_1 + \frac{1}{2}\vec{\Sigma}_{23} \times \vec{\Sigma}_{45}\right), \end{aligned} \tag{22}$$

where $\vec{\Sigma}_{45} = \vec{\sigma}_4 + \vec{\sigma}_5$. The representation of the Hamiltonian in Eq. (22) within the ground-state subspace spanned by $\{|g\mathcal{T}_-\mathcal{T}_-\rangle, |s\mathcal{T}_0\mathcal{T}_-\rangle, |s\mathcal{T}_-\mathcal{T}_0\rangle\}$ coincides with that presented in Eq. (15). Likewise, within the ground-state subspace spanned

TABLE I. Evolution directions of the quantum states versus time.

N/t	0	$\pi/3\sqrt{3}\kappa$	$2\pi/3\sqrt{3}\kappa$	$\pi/\sqrt{3}\kappa$
3	$\|gss\rangle$	$\|sgs\rangle$	$\|ssg\rangle$	$\|gss\rangle$
3	$\|sgg\rangle$	$\|ggs\rangle$	$\|gsg\rangle$	$\|sgg\rangle$
4	$\|g\mathcal{T}_-s\rangle$	$\|s\mathcal{T}_0s\rangle$	$\|s\mathcal{T}_-g\rangle$	$\|g\mathcal{T}_-s\rangle$
4	$\|s\mathcal{T}_+g\rangle$	$\|g\mathcal{T}_+s\rangle$	$\|g\mathcal{T}_0g\rangle$	$\|s\mathcal{T}_+g\rangle$
5	$\|g\mathcal{T}_-\mathcal{T}_-\rangle$	$\|s\mathcal{T}_0\mathcal{T}_-\rangle$	$\|s\mathcal{T}_-\mathcal{T}_0\rangle$	$\|g\mathcal{T}_-\mathcal{T}_-\rangle$
5	$\|s\mathcal{T}_+\mathcal{T}_+\rangle$	$\|g\mathcal{T}_+\mathcal{T}_0\rangle$	$\|g\mathcal{T}_0\mathcal{T}_+\rangle$	$\|s\mathcal{T}_+\mathcal{T}_+\rangle$
5	$\|gs\mathcal{Q}_{-3/2}\rangle$	$\|sg\mathcal{Q}_{-3/2}\rangle$	$\|ss\mathcal{Q}_{-1/2}\rangle$	$\|gs\mathcal{Q}_{-3/2}\rangle$
5	$\|sg\mathcal{Q}_{3/2}\rangle$	$\|gg\mathcal{Q}_{1/2}\rangle$	$\|gs\mathcal{Q}_{3/2}\rangle$	$\|sg\mathcal{Q}_{3/2}\rangle$

by $\{|s\mathcal{T}_+\mathcal{T}_+\rangle, |g\mathcal{T}_0\mathcal{T}_+\rangle, |g\mathcal{T}_+\mathcal{T}_0\rangle\}$, the time-evolution operator can be equivalently recast as $\hat{U}^\dagger(t)$.

Similarly, the second type can be regarded as the interaction of spin-$\frac{3}{2}$ particles with two spin-$\frac{1}{2}$ particles. If we initialize the phase to $\phi_1 = 2\pi/3$, $\phi_2 = 4\pi/3$, $\phi_3 = \phi_4 = \phi_5 = 2\pi$, $\Omega_1 = \Omega_2 = \Omega$, and $\Omega_3 = \Omega_4 = \Omega_5 = \Omega/\sqrt{3}$, the effective Hamiltonian can be written as

$$\hat{H}_{\text{eff}}^{(5,2)} = -\kappa\vec{e}_z \cdot \left(\vec{\sigma}_1\times\vec{\sigma}_2+\frac{1}{\sqrt{3}}\vec{\sigma}_2 \times \vec{\Sigma}_{345}+\frac{1}{\sqrt{3}}\vec{\Sigma}_{345} \times \vec{\sigma}_1\right), \tag{23}$$

where $\vec{\Sigma}_{345} = \vec{\sigma}_3 + \vec{\sigma}_4 + \vec{\sigma}_5$. For this situation, we represent the quantum state using a quartet denotation, where

$$\begin{aligned}
|\mathcal{Q}_{-3/2}\rangle &= |sss\rangle,\\
|\mathcal{Q}_{-1/2}\rangle &= \frac{1}{\sqrt{3}}(|gss\rangle + |sgs\rangle + |ssg\rangle),\\
|\mathcal{Q}_{+1/2}\rangle &= \frac{1}{\sqrt{3}}(|sgg\rangle + |gsg\rangle + |ggs\rangle),\\
|\mathcal{Q}_{+3/2}\rangle &= |ggg\rangle.
\end{aligned}$$

Similar to the previous discussion, the form of the Hamiltonian in Eq. (23) within the ground-state subspace spanned by $\{|gs\mathcal{Q}_{-3/2}\rangle, |sg\mathcal{Q}_{-3/2}\rangle, |ss\mathcal{Q}_{-1/2}\rangle\}$ is given by Eq. (15). Additionally, the time-evolution operator in the other subspace spanned by $\{|sg\mathcal{Q}_{3/2}\rangle, |gs\mathcal{Q}_{3/2}\rangle, |gg\mathcal{Q}_{1/2}\rangle\}$ can be represented as $\hat{U}^\dagger$. To summarize, the evolution directions of the three-state chiral current are shown in Table I.

C. Multistate chiral current

In addition to the aforementioned dynamical evolution, we also modulate the third type of phase distribution with $\phi_k = -2k\pi/5$. The corresponding effective Hamiltonian reads

$$\hat{H}_{\text{eff}}^{(5,3)} = \kappa_1\hat{o}_1 + \kappa_2\hat{o}_2, \tag{24}$$

where

$$\hat{o}_1 = \sum_{k=1}^{5}\vec{e}_z \cdot (\vec{\sigma}_k \times \vec{\sigma}_{k+1}), \tag{25a}$$

$$\hat{o}_2 = \sum_{k=1}^{5}\vec{e}_z \cdot (\vec{\sigma}_k \times \vec{\sigma}_{k+2}). \tag{25b}$$

Here we employ the periodic boundary condition, which implies $k \equiv k \bmod N$. The Hamiltonian in Eq. (24) contains both nearest-neighbor and next-nearest-neighbor terms. Indeed, it is necessary to satisfy the condition $\kappa_2/\kappa_1 = \sqrt{5} - 2 \approx 0.2361$ [24]; we can obtain the perfect ground-state chiral current in this situation. Subsequently, we will proceed with a brief analysis of its dynamical process.

In the ground-state subspace spanned by $\{|gssss\rangle, |sgsss\rangle, |ssgss\rangle, |sssgs\rangle, |ssssg\rangle\}$, the Hamiltonian in Eq. (24) is represented as

$$\hat{H}_{\text{sub}}^{(5,3)} = \frac{i}{2}\begin{pmatrix} 0 & \kappa_1 & \kappa_2 & -\kappa_2 & -\kappa_1 \\ -\kappa_1 & 0 & \kappa_1 & \kappa_2 & -\kappa_2 \\ -\kappa_2 & -\kappa_1 & 0 & \kappa_1 & \kappa_2 \\ \kappa_2 & -\kappa_2 & -\kappa_1 & 0 & \kappa_1 \\ \kappa_1 & \kappa_2 & -\kappa_2 & -\kappa_1 & 0 \end{pmatrix}. \tag{26}$$

The eigenvalues for $\hat{H}_{\text{eff}}^{(5,3)}$ are $\{0, \pm\omega, \pm3\omega\}$ with $\omega = \sqrt{5-2\sqrt{5}}\kappa_1/2 \approx 0.3633\kappa_1$. Accordingly, the time-evolution operator can be recast as

$$\hat{U}'(t) = \begin{pmatrix} y_1(t) & y_5(t) & y_4(t) & y_3(t) & y_2(t) \\ y_2(t) & y_1(t) & y_5(t) & y_4(t) & y_3(t) \\ y_3(t) & y_2(t) & y_1(t) & y_5(t) & y_4(t) \\ y_4(t) & y_3(t) & y_2(t) & y_1(t) & y_5(t) \\ y_5(t) & y_4(t) & y_3(t) & y_2(t) & y_1(t) \end{pmatrix}, \tag{27}$$

where

$$\begin{aligned}
y_1(t) &= \tfrac{1}{5}[1 + 4\cos(2\omega t)\cos(\omega t)],\\
y_2(t) &= \tfrac{1}{5}\left[1 + 4\cos\left(2\omega t + \tfrac{3}{5}\pi\right)\cos\left(\omega t - \tfrac{1}{5}\pi\right)\right],\\
y_3(t) &= \tfrac{1}{5}\left[1 + 4\cos\left(2\omega t + \tfrac{1}{5}\pi\right)\cos\left(\omega t + \tfrac{3}{5}\pi\right)\right],\\
y_4(t) &= \tfrac{1}{5}\left[1 + 4\cos\left(2\omega t + \tfrac{4}{5}\pi\right)\cos\left(\omega t + \tfrac{2}{5}\pi\right)\right],\\
y_5(t) &= \tfrac{1}{5}\left[1 + 4\cos\left(2\omega t + \tfrac{7}{5}\pi\right)\cos\left(\omega t + \tfrac{1}{5}\pi\right)\right].
\end{aligned} \tag{28}$$

When the initial state is $|gssss\rangle$, the evolution state reads

$$\begin{aligned}
|\psi(t)\rangle = {}& y_1(t)|gssss\rangle + y_2(t)|sgsss\rangle + y_3(t)|ssgss\rangle\\
&+ y_4(t)|sssgs\rangle + y_5(t)|ssssg\rangle.
\end{aligned} \tag{29}$$

When the evolution time $t = 0, 2\pi/5\omega, 4\pi/5\omega, 6\pi/5\omega, 8\pi/5\omega, 2\pi/\omega$, the evolution state $|\psi(t)\rangle = |gssss\rangle, |ssgss\rangle, |sssgs\rangle, |sgsss\rangle, |ssgss\rangle, |gssss\rangle$, respectively. The ground state $|g\rangle$ traverses the ring sites in the direction of $1 \to 3 \to 5 \to 2 \to 4 \to 1 \to \cdots$ within one period of $T = 2\pi/\omega$. In the ground-state subspace spanned by $\{|sgggg\rangle, |gsggg\rangle, |ggsgg\rangle, |gggsg\rangle, |ggggs\rangle\}$, the time-evolution operator, denoted by $\hat{U}'^\dagger(t)$, gives rise to the opposite evolution direction, i.e., $1 \to 4 \to 2 \to 5 \to 3 \to 1 \to \cdots$.

For the case $\varepsilon/\nu = 2.4048$, the effective coupling constants in the Hamiltonian in Eq. (24) can be reduced to

$$\begin{aligned}
\kappa_1 &= \frac{\Omega^2 g^2}{4\Delta^2\nu}\sum_{n=1}^{\infty}\mathcal{J}_n^2\left(\frac{\varepsilon}{\nu}\right)\sin\left(\frac{2n\pi}{5}\right)\Big/n,\\
\kappa_2 &= \frac{\Omega^2 g^2}{4\Delta^2\nu}\sum_{n=1}^{\infty}\mathcal{J}_n^2\left(\frac{\varepsilon}{\nu}\right)\sin\left(\frac{4n\pi}{5}\right)\Big/n,
\end{aligned} \tag{30}$$

with $\Omega_k = \Omega$ and $\Delta_k = \Delta$. Unfortunately, the ratio of the coupling constant κ_2/κ_1 for such a specific case is 0.2702, so we can obtain the imperfect ground-state chirality, which will be illustrated numerically in Sec. III B.

III. NUMERICAL SIMULATION OF GROUND-STATE CHIRAL CURRENT, RANGE OF APPLICABILITY, AND POTENTIAL EXPERIMENTAL POSSIBILITY

In this section we provide the effective master equation involving only the ground-state manifold, and the numerical simulation results continue to show that ground-state chiral current can be reliably achieved. Subsequently, we also provide a detailed explanation for the effective conditions of our model and its potential experimental possibility.

A. Effective master equation

For weakly driven atoms, the evolution and decay of the excited states occur on a timescale that is significantly faster than any other timescale in the system. The separation of the Hilbert space into rapidly and slowly evolving ground and excited states has been explored by non-Hermitian Hamiltonians. Specifically, for a coupling of the ground to the excited states much weaker than the evolution inside the subspaces, a formalism for effective processes can be established by extending the Feshbach projection-operator approach [78,79]. By combining perturbation theory of the density operator and adiabatic elimination of the excited states, we reduce the dynamics to an effective master equation involving only the ground-state manifold (more details are reported in the Appendix)

$$\begin{aligned}\frac{d\hat{\rho}}{dt} &= -i[\hat{H}_{\rm eff}(t),\hat{\rho}] + \gamma_1\hat{a}\hat{\rho}\hat{a}^\dagger - \frac{\gamma_1}{2}\{\hat{a}^\dagger\hat{a},\hat{\rho}\} \\ &+ \sum_k \hat{\mathcal{L}}^{\rm eff}_{k,gs}(t)\hat{\rho}\big[\hat{\mathcal{L}}^{\rm eff}_{k,gs}(t)\big]^\dagger - \tfrac{1}{2}\big\{\big[\hat{\mathcal{L}}^{\rm eff}_{k,gs}(t)\big]^\dagger\hat{\mathcal{L}}^{\rm eff}_{k,gs}(t),\hat{\rho}\big\} \\ &+ \sum_k \hat{\mathcal{L}}^{\rm eff}_{k,sg}(t)\hat{\rho}\big[\hat{\mathcal{L}}^{\rm eff}_{k,sg}(t)\big]^\dagger - \tfrac{1}{2}\big\{\big[\hat{\mathcal{L}}^{\rm eff}_{k,sg}(t)\big]^\dagger\hat{\mathcal{L}}^{\rm eff}_{k,sg}(t),\hat{\rho}\big\}.\end{aligned} \tag{31}$$

Here $\{\hat{A},\hat{B}\}\equiv\hat{A}\hat{B}+\hat{B}\hat{A}$ represents the anticommutator of operators $\hat{A}$ and $\hat{B}$ and the effective Hamiltonian is given by

$$\hat{H}_{\rm eff}(t) = \hat{H}'_0(t) + \hat{H}'_{\rm int}(t), \tag{32}$$

where

$$\begin{aligned}\hat{H}'_0(t) &= \sum_k\left(\varepsilon_k\cos(\nu_k t-\phi_k) - \frac{4g^2\Delta_k}{4\Delta_k^2+\gamma_2^2}\hat{a}^\dagger\hat{a}\right)\hat{\sigma}_k^{gg} \\ &- \frac{\Delta_k\Omega_k^2}{4\Delta_k^2+\gamma_2^2}\hat{\sigma}_k^{ss}, \\ \hat{H}'_{\rm int}(t) &= -\sum_k\frac{2g\Delta_k\Omega_k e^{i(\bar{\Delta}'-\Delta_k)t}}{4\Delta_k^2+\gamma_2^2}\hat{a}\hat{\sigma}_k^{sg} + \text{H.c.}\end{aligned} \tag{33}$$

Despite the presence of complex terms in the effective Hamiltonian, it contains two Stark shift terms and an effective two-photon transition between the two ground states. In the absence of dissipative processes ($\gamma_2=0$), this effective Hamiltonian can be degenerated into Eq. (6). Furthermore, we derive the effective Lindblad operators

$$\hat{\mathcal{L}}^{\rm eff}_{k,gs}(t) = \sqrt{\frac{\gamma_2}{2}}\left(\frac{\Omega_k}{2\tilde{\Delta}_k}\hat{\sigma}_k^{gs} + \frac{ge^{i(\bar{\Delta}'-\Delta_k)t}}{\tilde{\Delta}_k}\hat{a}\hat{\sigma}_k^{gg}\right),$$

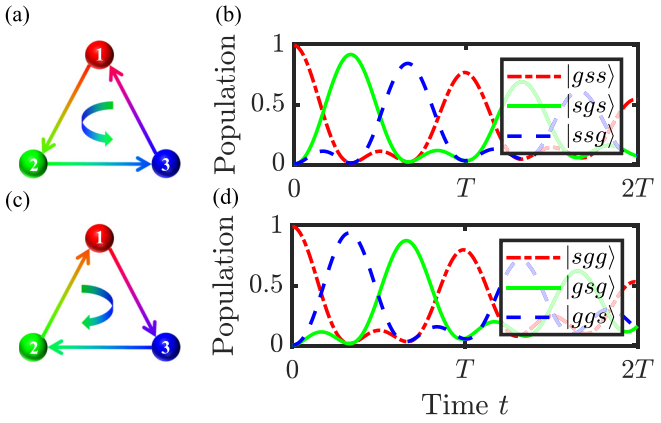

FIG. 2. Schematic and population diagrams illustrating the evolution of chirality versus time generated from the states $|gss\rangle$ and $|sgg\rangle$ along the counterclockwise and the clockwise directions, respectively. The dynamics is governed by the Hamiltonian in Eq. (31) and the other parameters are $\Omega_k = 1.2g$, $\nu_k = g$, $\varepsilon_k = 2.4048g$, $\bar{\Delta}' = 50g$, $\Delta_k = \bar{\Delta}' - \Omega_k^2/4\bar{\Delta}'$, and $\gamma_1 = \gamma_2 = 0.01g$.

$$\hat{\mathcal{L}}^{\rm eff}_{k,sg}(t) = \sqrt{\frac{\gamma_2}{2}}\left(\frac{\Omega_k}{2\tilde{\Delta}_k}\hat{\sigma}_k^{ss} + \frac{ge^{i(\bar{\Delta}'-\Delta_k)t}}{\tilde{\Delta}_k}\hat{a}\hat{\sigma}_k^{sg}\right), \tag{34}$$

with $\tilde{\Delta}_k = \Delta_k - i\gamma_2/2$. In addition to featuring a loop-term corresponding to each ground state within this configuration, these operators incorporate effective decays from one ground state to the other. Thus, we note that, depending on the relative strength of the effective quantities, the resulting effective dynamics will be governed by either coherent or decoherent behavior, which will be illustrated specifically in Sec. III C.

B. Numerical simulation of three-state and multistate chirality

Floquet engineering is a typical strategy for controlling long-term system dynamics, characterized by periodically modulating the system frequency to synthesize the target Hamiltonian [48]. Theoretical studies have demonstrated that Floquet modulation can be employed to generate arbitrary two-body spin interactions [80,81]. By periodically adjusting the system parameters, we have successfully synthesized the z component of the DMI. Moving forward, we conduct numerical simulations to investigate the chiral dynamics involving three, four, and five atoms. In what follows, we first present an example of three atoms arranged in a triangular loop to discuss the chiral current with initial state $|gss\rangle$. We provide numerical simulations based on the Hamiltonian (31) and present the chiral dynamics depicted in Figs. 2(a) and 2(b). The results reveal an interesting dynamical pattern: The state $|g\rangle$ injected into one of the sites flows counterclockwise through the three-atom sites. Such a phenomenon totally aligns with previous theoretical prediction. Furthermore, when considering $|sgg\rangle$ as the initial state, the transfer of the state $|s\rangle$ follows the clockwise rotation $1\to3\to2\to1\to\cdots$ in Figs. 2(c) and 2(d). More remarkably, the initial-state flip causes the opposite direction of chiral evolution, which can be attributed to the preservation of time-reversal symmetry by the z component of DMI. The abundance of phases affords us the opportunity to witness a diverse range of chiral dynamics across

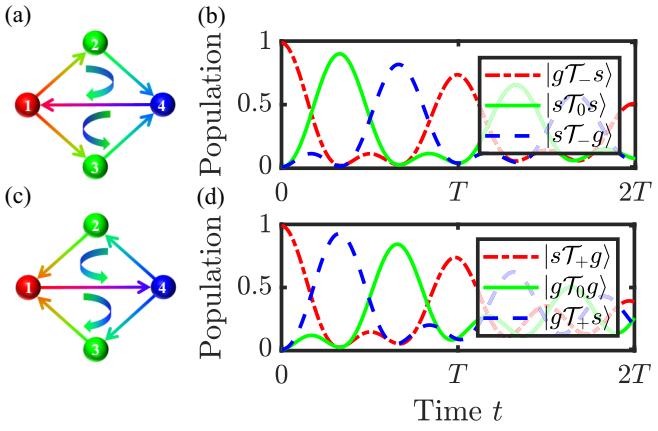

FIG. 3. Schematic and population diagrams illustrating the evolution of chirality versus time generated from the states $|g\mathcal{T}_-s\rangle$ and $|s\mathcal{T}_+g\rangle$, respectively. The dynamics is governed by the Hamiltonian in Eq. (31) and the other parameters are $\nu_k = g$, $\varepsilon_k = 2.4048g$, $\Omega_{1,4} = 1.2g$, $\Omega_{2,3} = 1.2g/\sqrt{2}$, $\bar{\Delta}' = 50g$, $\Delta_k = \bar{\Delta}' - \Omega_k^2/4\bar{\Delta}'$, and $\gamma_1 = \gamma_2 = 0.01g$.

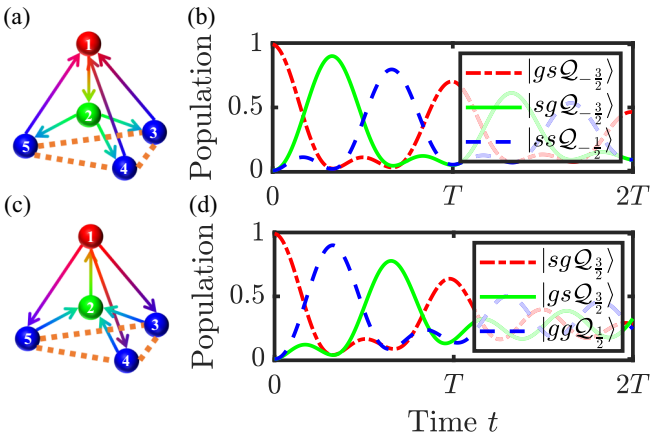

FIG. 5. Schematic and population diagrams illustrating the evolution of chirality versus time generated from the states $|gs\mathcal{Q}_{-3/2}\rangle$ and $|sg\mathcal{Q}_{3/2}\rangle$, respectively. The dynamics is governed by the Hamiltonian in Eq. (31) and the other parameters are $\Omega_{1,2} = 1.2g$, $\Omega_{3,4,5} = 1.2g/\sqrt{3}$, $\nu_k = g$, $\varepsilon_k = 2.4048g$, $\bar{\Delta}' = 50g$, $\Delta_k = \bar{\Delta}' - \Omega_k^2/4\bar{\Delta}'$, and $\gamma_1 = \gamma_2 = 0.01g$.

multiple atoms. In Fig. 3 we illustrate the population transfer of four atoms. Obviously, the numerical results for the initial states $|g\mathcal{T}_-s\rangle$ and $|s\mathcal{T}_+g\rangle$ exhibit the opposite chirality. In other words, when the initial state is $|g\mathcal{T}_-s\rangle$, the evolutionary path of the state $|g\rangle$ follows a sequence of $1 \to \{2,3\} \to 4 \to 1 \to \cdots$. Otherwise, the state $|s\rangle$ circulates along the route $1 \to 4 \to \{2,3\} \to 1 \to \cdots$ in the scenario of flipping the initial state.

For the case of five atoms, three distinct phase distributions were selected in Sec. II. The first one closely resembles the previous distribution, and the corresponding evolutionary outcomes are illustrated in Fig. 4. It can be perceived that the state $|g\rangle$ traverses the sites in a counterclockwise manner. In other words, the site 1 advances to the superposition of sites 2 and 3, then progresses to the superposition of sites 4 and 5, and ultimately goes back to site 1. For another scenario, the

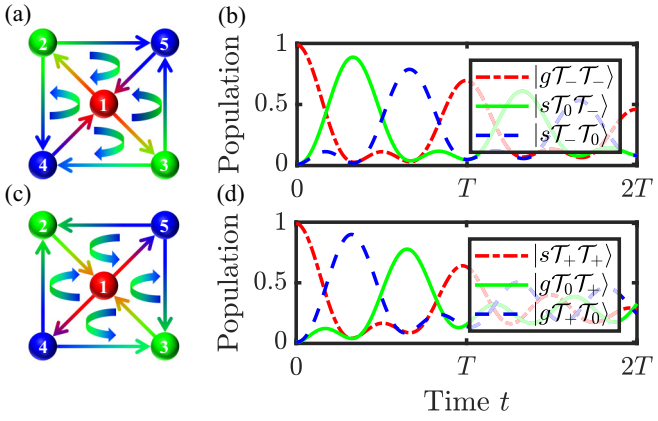

FIG. 4. Schematic and population diagrams illustrating the evolution of chirality versus time generated from the states $|g\mathcal{T}_-\mathcal{T}_-\rangle$ and $|s\mathcal{T}_+\mathcal{T}_+\rangle$, respectively. The dynamics is governed by the Hamiltonian in Eq. (31) and the other parameters are $\nu_k = g$, $\varepsilon_k = 2.4048g$, $\Omega_1 = 1.2g$, $\Omega_{2,3,4,5} = 1.2g/\sqrt{2}$, $\bar{\Delta}' = 50g$, $\Delta_k = \bar{\Delta}' - \Omega_k^2/4\bar{\Delta}'$, and $\gamma_1 = \gamma_2 = 0.01g$.

state $|s\rangle$ follows the opposite trajectory. It commences from site 1, then passes through the superposition of sites 4 and 5, transfers to the superposition of sites 2 and 3, and eventually returns to site 1. As mentioned earlier, the second type of phase modulation follows a similar principle, which can be clearly seen from Fig. 5. When the system is initialized to the state $|gs\mathcal{Q}_{-3/2}\rangle$, the chiral current evolves along a specific path $1 \to 2 \to \{3,4,5\} \to 1 \to \cdots$. In another situation, the direction of evolution changes as $1 \to \{3,4,5\} \to 2 \to 1 \to \cdots$. The above are the numerical simulation results for the three-state chiral current, where it is clearly shown that the chirality emerges from the $2\pi/3$ phase shift between the three different populations oscillations. Consequently, summarizing the results from the analysis above, our scheme is reasonable to open up exciting possibilities for arbitrary atom numbers N and shows that the transfer period remains exactly independent of the choice of N. Nevertheless, the third kind of phase modulation exhibits a consistent phase difference between adjacent lattice sites in Fig. 6. The dynamics is driven by the Hamiltonian in Eq. (31), and the state $|g\rangle$ traverses the sites in the direction of $1 \to 3 \to 5 \to 2 \to 4 \to 1 \to \cdots$. Significantly, the maximum population approaches 1, which explains the coupling strength between the nearest-neighbor and next-nearest-neighbor items not being absolutely proportional. Accordingly, combined with the other initial state, the propagation direction of the chiral current will be reversed. Our finding reveals that the spin dynamics driven by the z component of DMI exhibits a chiral evolution phenomenon. As a result, multiple instances of chiral motions are realized within various atomic configurations. In particular, reversing the initial state of all sites, the chiral evolution is in the opposite direction, yet this does not affect the time for completing a full cycle.

C. Range of applicability and potential experimental possibility

Building upon the preceding content, we have obtained the effective master equation by eliminating the high-energy

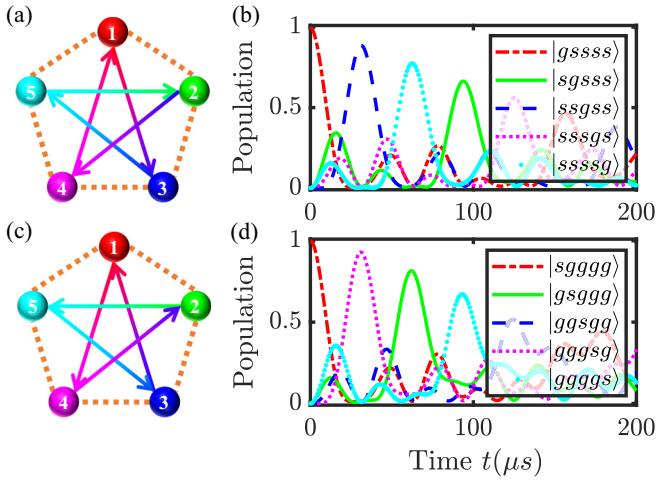

FIG. 6. Schematic and population diagrams illustrating the evolution of chirality versus time generated from the states $|gssss\rangle$ and $|sgggg\rangle$, respectively. The dynamics is governed by the Hamiltonian in Eq. (31) and the other parameters are $\Omega_k = 1.2g$, $\nu_k = g$, $\varepsilon_k = 2.4048g$, $\bar{\Delta}' = 50g$, $\Delta_k = \bar{\Delta}' - \Omega_k^2/4\bar{\Delta}'$, and $\gamma_1 = \gamma_2 = 0.01g$.

level. It is crucial to emphasize that our model and approach are applicable within a specific range. In this section we provide a detailed explanation for the effective conditions of the model and its potential experimental possibility.

1. Decoherence and spontaneous emission

Our model seeks to analyze the transmission process of spin chirality currents in driven three-level Λ-configuration atoms. The precision of effective results may give rise to optimization under conditions of low spontaneous emission rates. While such a model exhibits significant capabilities for specialized systems, it still possesses certain limitations. One limitation is that a high atomic spontaneous emission could wash out the effective coupling, thereby the effective Hamiltonian no longer accurately reporting the dynamical evolution. In Figs. 7(a), 7(c), and 7(e) we employ comparative realistic spontaneous emission to simulate chiral current, which indicates that the process of perfect quantum state transfer becomes impractical over time. In order to evaluate the atomic spontaneous emission, we introduce the corresponding population of the subspace as $P_{\text{sub}} = P_{|gss\rangle} + P_{|sgs\rangle} + P_{|ssg\rangle}$. In particular, once inserted with its actual experimental linewidth, ^{87}Rb, satisfying $\gamma_2 \approx g/20$, is not applied to achieve optimal chiral dynamics. Actually, the atomic spontaneous radiation disrupts the conserved layout of atoms within the corresponding subspace and eventually transforms back into the ground state based on the effective dissipation operator from Eq. (34). This situation reveals that introducing atoms or ions with longer excited lifetimes could improve the efficiency of the quantum information process. On the other hand, the tolerance for cavity losses is indeed a critical aspect to consider, especially the discussion of the impact of spontaneous emission on the proposed effect. To assess whether the current technology meets the acceptable level of cavity losses, further analysis and experimentation are necessary to determine the practical feasibility of achieving the desired

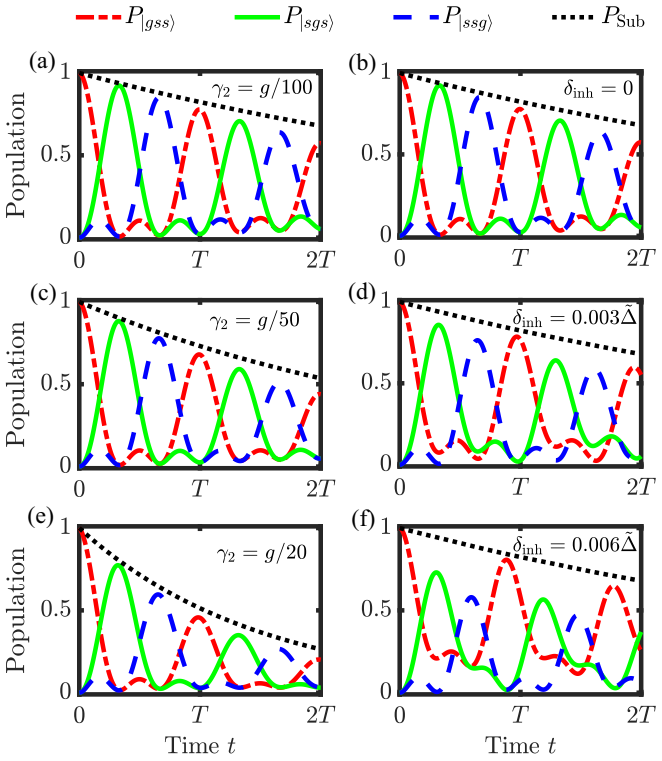

FIG. 7. Evolution of chirality versus time generated from the states $|gss\rangle$ under the conditions of (a), (c), and (e) a fixed cavity decay rate $\gamma_1 = 0.01g$ and varying spontaneous emission rates and (b), (d), and (f) a fixed dissipative rates $\gamma_1 = \gamma_2 = 0.01g$ and varying heterogeneous detunings. The dynamics is governed by the Hamiltonian in Eq. (31) and the other parameters are $\Omega_k = 1.2g$, $\nu_k = g$, $\varepsilon_k = 2.4048g$, $\bar{\Delta}' = 50g$, $\Delta_k = \bar{\Delta}' - \Omega_k^2/4\bar{\Delta}'$, and $\tilde{\Delta} = (\Delta_1 + \Delta_2 + \Delta_3)/3$.

cavity performance within existing technological constraints [82,83]. Combining stable cavity photons or low dissipative rate, the average photons are introduced to examine the impact of cavity losses on the chiral current [84]. We conclude that the average photon number throughout the evolution is approximately 10^{-4}, which exerts minimal influence on the dynamics compared to the distributed probabilities of other configurations.

2. Ensemble nonuniformity

In the preceding section we assumed that the frequency of each atomic excitation remains identical. However, the atoms may possess diverse levels in the ensemble, which leads to a discrepancy in the corresponding detuning. In other words, the uncertainty in the ensemble and parameters diminishes the impact of the effective coupling. In order to illustrate the effect of ensemble nonuniformities, we regard three different atoms as an example to show the evolution of chiral current under the condition of relatively heterogeneous detuning, where such heterogeneity is denoted by $(\Delta_1 + \delta_{\text{inh}}, \Delta_2, \Delta_3 - \delta_{\text{inh}})$. In Figs. 7(b), 7(d), and 7(f) we readily observe that a rise in relative nonuniform deviations triggers strong oscillations in the dynamical evolution within the subspace, thus disrupting the chiral current to a certain degree. Such a phenomenon implies that signatures of the chiral current can be observed

even for realistic ^{87}Rb parameters. On the other hand, similar to the aforementioned uneven detuning, we also consider the systematic errors raised by the nonequal coupling strengths, namely, $g+\delta_g$, g, and $g-\delta_g$, where δ_g represents the magnitude of the error. Since the effective strength relies on the coupling g, its lack of uniformity triggers significant oscillatory effects on the corresponding chiral current. Consequently, it is to be expected that the fidelity of the chiral current will diminish as the deviation of the coupling strength increases. Given these factors, maximizing the uniformity of the ensemble can enhance the reliability of our scheme to the greatest extent possible.

3. Potential experimental possibility

Based on previous work [31–34,85,86], we investigate the spin dynamics of trapped ^{87}Rb atoms in a single-mode optical resonator. The conduit for mediating interactions from the $|S_{1/2}\rangle \rightarrow |P_{3/2}\rangle$ transitions is a 780.02-nm cavity mode at detuning as high as several tens of gigahertz [58]. The energy-level splitting of the hyperfine structure between levels $|S_{1/2}, F=2\rangle$ and $|S_{1/2}, F=1\rangle$ is approximately 6834.68 MHz, i.e., $\omega_g/2\pi \approx 6834.68$ MHz. The carrier frequency ω_k^L is roughly equal to 384.225 THz [56]. As a result, the other corresponding parameters could uniformly be chosen as $\omega_e/2\pi \approx 384.23$ THz, $\omega_c/2\pi \approx 384.22$ THz, $\Delta_k/2\pi \approx 5000$ MHz, $\Omega_k/2\pi \approx 120$ MHz, $g/2\pi \approx 100$ MHz, and $\nu_k/2\pi \approx 100$ MHz. The decay rates of the cavity are $\gamma_1/2\pi \approx 1$ MHz [84] and $\gamma_2/2\pi \approx 6.1$ MHz. Thus, all the necessary conditions for achieving effective dynamics have been successfully satisfied. However, it is worth mentioning that similar to Fig. 7(e), the curve generated with the aforementioned experimental parameters can indeed exhibit the characteristics of chiral current, yet it falls short of achieving a perfect quantum state transfer process. To optimize this process, it is necessary to select atoms with longer lifetimes. We may consider several nitrogen-vacancy (NV) centers coupled to a common superconducting coplanar waveguide resonator with the hyperfine ground state, with the distance between NV centers placed in close proximity, which could feasibly facilitate the coupling between the quantum field and atoms. On the other hand, the NV centers exhibit extended coherence times and remarkable quantum controllability [87–89], e.g., the spin relaxation time under room-temperature conditions satisfies our criteria [90] and extends even longer at lower temperatures [91], while the electron-spin relaxation time for a NV center could reach up to 10 ms ($\gamma_2 = 0.01$ MHz) at low temperature under an appropriately chosen magnetic field for our system [92]. Once the condition of the parameter could be fulfilled, the large-detuning regime and high-frequency expansion approximation ensure the relatively perfect chiral current. Certainly, we also consider the Rydberg atoms to achieve the desired dynamics. Perhaps the Rydberg state could serve as the excited state. However, we must ensure the restriction of the distance between atoms beyond the blockade radius to safely omit the interaction between atoms. Under the condition where the driving frequency is significantly lower than the strength of the blockade interaction, only one atom can be excited to the Rydberg state within a system of N driven Rydberg atoms. Such a situation enables us to label the excited atom as occupying the first position, with any atoms in the ground state occupying the second position. Naturally, we can regard the remaining atoms as a collective Rydberg superatom [93], thereby facilitating the realization of triangular chiral current in diverse directions. Even in cases where interactions exist among Rydberg atoms, it is crucial to highlight in the literature that effective master equations could be derived with the adiabatic elimination of the excited states and second-order perturbation theory. Fortunately, owing to the comparatively extended lifetime of Rydberg levels, a low dissipation rate guarantees the chiral evolution within a secure zone, ultimately facilitating the achievement of the desired dynamics.

IV. CONCLUSION

To summarize, we simulated the DMI and chiral current in atomic manifolds via periodic modulation. Utilizing a three-level system in a Λ configuration, we derived an effective Hamiltonian for the ground-state subspace via adiabatic elimination. By simultaneously modulating the driving frequencies and initial phases, we achieved various configurations of the DMI for different ground-state chiral dynamics, including three-state and multistate chiral currents. The numerical simulation results further confirmed that the proposed method is capable of generating the ground-state chiral current. Furthermore, we discussed in detail the effects of adverse factors on the chiral current. We found that the experimental operability opens up possibilities for reliable quantum state transfer. Our proposal of three-state chiral current can be extended to arbitrary atom numbers, and it is possible to realize the perfect multistate chiral current by considering a more tunable interaction between further neighbors. On the other hand, we have recognized that nonuniformity disrupts the effect of chiral current. However, the deeper dynamics underlying this scenario and strategies to mitigate the oscillation effect remain thought-provoking questions for future research in chiral dynamics. Additionally, the phenomena of chiral current occurring in curved spaces and nonflat manifolds may give rise to new quantum effects resembling the Berry phase and anomalous Hall effect, which are crucial for understanding the fundamental principles of quantum mechanics and driving the development of advanced quantum devices. By harnessing the behavior of spin chiral current on manifolds with varying geometric structures, we can design and implement more sophisticated and diverse quantum information processing devices, ultimately boosting the efficiency and fault tolerance of quantum information processing.

ACKNOWLEDGMENTS

The authors thank the anonymous reviewers for constructive comments that helped improve the quality of this paper. The work was supported by the Natural Science Foundation of Jilin Province (Grant No. JJKH20190279KJ) and the Key Laboratory of Advanced Optical Manufacturing Technologies of Jiangsu Province, Soochow University (Grant No. KJS2336). C.W. was supported by the National Research Foundation, Singapore and A*STAR under its Quantum Engineering Programme (NRF2021-QEP2-02-P03). C.S. was

supported by the Plan for Science and Technology Development of Jilin Province (Grant No. 20240101315JC) and the scientific research project of the Education Department of Jilin Province (Grant No. JJKH20231293KJ).

APPENDIX: EFFECTIVE OPERATOR FORMALISM FOR MASTER EQUATION

When incorporating decoherence into the system, non-Hermitian Hamiltonians are frequently utilized to characterize the dynamics of open systems, which can be formulated more rigorously through the so-called quantum jump theory or Monte Carlo wave-function method. Open systems also exhibit distinct timescales associated with different effects such that the Hilbert space can be divided into two parts, one for the rapidly decaying (excited) states and another for the relatively stable (ground) states. Next we show how to obtain an effective master-equation formalism between ground-ground states by introducing adiabatic elimination. For our system, we consider the effects of atomic spontaneous emission by assuming that the excited state $|e\rangle$ decays into the ground states $|g\rangle$ and $|s\rangle$ with the same spontaneous emission rate. Therefore, the dynamics of the system can be described by the Markovian master equation

$$\begin{aligned}\frac{d\hat{\rho}}{dt} &= -i[\hat{\tilde{H}}(t),\hat{\rho}] + \gamma_1\hat{a}\hat{\rho}\hat{a}^\dagger - \frac{\gamma_1}{2}\{\hat{a}^\dagger\hat{a},\hat{\rho}\} \\ &+ \sum_k \hat{\mathcal{L}}_{gs}^{(k)}\hat{\rho}\big[\hat{\mathcal{L}}_{gs}^{(k)}\big]^\dagger - \tfrac{1}{2}\big\{\big[\hat{\mathcal{L}}_{gs}^{(k)}\big]^\dagger\hat{\mathcal{L}}_{gs}^{(k)},\hat{\rho}\big\} \\ &+ \sum_k \hat{\mathcal{L}}_{sg}^{(k)}\hat{\rho}\big[\hat{\mathcal{L}}_{sg}^{(k)}\big]^\dagger - \tfrac{1}{2}\big\{\big[\hat{\mathcal{L}}_{sg}^{(k)}\big]^\dagger\hat{\mathcal{L}}_{sg}^{(k)},\hat{\rho}\big\}, \end{aligned} \tag{A1}$$

where the dissipative operators are given as

$$\hat{\mathcal{L}}_{gs}^{(k)} = \sqrt{\gamma_2/2}|g_k\rangle\langle e_k|, \quad \hat{\mathcal{L}}_{sg}^{(k)} = \sqrt{\gamma_2/2}|s_k\rangle\langle e_k|.$$

In order to distinguish the non-Hermitian Hamiltonian of the excited states, we introduce $\hat{H}_{\rm NH}$ to Eq. (A1) and obtain a reduced master equation

$$\begin{aligned}\frac{d\hat{\rho}}{dt} &= -i\{(\hat{H}_{\rm NH}+\hat{H}_g+\hat{V})\hat{\rho} - \hat{\rho}([\hat{H}_{\rm NH}]^\dagger+\hat{H}_g+\hat{V})\} \\ &+ \sum_k \hat{\mathcal{L}}_{gs}^{(k)}\hat{\rho}\big[\hat{\mathcal{L}}_{gs}^{(k)}\big]^\dagger + \hat{\mathcal{L}}_{sg}^{(k)}\hat{\rho}\big[\hat{\mathcal{L}}_{sg}^{(k)}\big]^\dagger \\ &+ \gamma_1\hat{a}\hat{\rho}\hat{a}^\dagger - \frac{\gamma_1}{2}\{\hat{a}^\dagger\hat{a},\hat{\rho}\}, \end{aligned} \tag{A2}$$

where $\hat{V} \equiv \hat{V}^+ + \hat{V}^-$. The $\hat{V}^+$ and $\hat{V}^-$ denote the perturbative excitations and deexcitations, respectively, of the system with $(\hat{V}^+)^\dagger = \hat{V}^-$, and $\hat{H}_g(t)$ is the ground-state Hamiltonian. In addition, $\hat{H}_{\rm NH} = \hat{H}_e - i/2\sum_k(\hat{\mathcal{L}}_{gs}^{(k)})^\dagger\hat{\mathcal{L}}_{gs}^{(k)} + (\hat{\mathcal{L}}_{sg}^{(k)})^\dagger\hat{\mathcal{L}}_{sg}^{(k)}$ represents the non-Hermitian Hamiltonian of the quantum jump formalism within $\hat{H}_e = \sum_k \Delta_k\hat{\sigma}_k^{ee}$, which is the Hamiltonian in the excited-state manifold. Considering our specific condition, the corresponding operations can be recast as

$$\begin{aligned}\hat{V}^+(t) &= \sum_k \frac{\Omega_k}{2}\hat{\sigma}_k^{es} + g\hat{a}e^{i(\bar{\Delta}'-\Delta_k)t}\hat{\sigma}_k^{eg}, \\ \hat{H}_g(t) &= \sum_k \varepsilon_k\cos(\nu_k t-\phi_k)\hat{\sigma}_k^{gg}, \\ \hat{H}_{\rm NH} &= \hat{H}_e - \frac{i}{2}\sum_k\big(\hat{\mathcal{L}}_{gs}^{(k)}\big)^\dagger\hat{\mathcal{L}}_{gs}^{(k)} + \big(\hat{\mathcal{L}}_{sg}^{(k)}\big)^\dagger\hat{\mathcal{L}}_{sg}^{(k)}. \end{aligned} \tag{A3}$$

According to the work in Ref. [79], adiabatically eliminating the excited state $|e\rangle$ results in the effective Hamiltonian and Lindblad operator in the ground-state subspace

$$\begin{aligned}\hat{H}_{\rm eff}(t) &= -\tfrac{1}{2}\hat{V}^-(t)([\hat{H}_{\rm NH}]^{-1}+{\rm H.c.})\hat{V}^+(t) + \hat{H}_g(t), \\ \hat{\mathcal{L}}_{k,gs}^{\rm eff}(t) &= \hat{\mathcal{L}}_{gs}^{(k)}[\hat{H}_{\rm NH}]^{-1}\hat{V}^+(t), \\ \hat{\mathcal{L}}_{k,sg}^{\rm eff}(t) &= \hat{\mathcal{L}}_{sg}^{(k)}[\hat{H}_{\rm NH}]^{-1}\hat{V}^+(t). \end{aligned} \tag{A4}$$

Taking our specific system into account and substituting the previous resonance condition $\bar{\Delta}' = \Delta_k + \Omega_k^2/4\Delta_k$ into Eq. (A4), we can derive the specific forms of the effective Hamiltonian and Lindblad operator as

$$\hat{H}_{\rm eff}(t) = \hat{H}_0'(t) + \hat{H}_{\rm int}'(t), \tag{A5}$$

where

$$\begin{aligned}\hat{H}_0'(t) &= \sum_k\left(\varepsilon_k\cos(\nu_k t-\phi_k) - \frac{4g^2\Delta_k}{4\Delta_k^2+\gamma_2^2}\hat{a}^\dagger\hat{a}\right)\hat{\sigma}_k^{gg} \\ &- \frac{\Delta_k\Omega_k^2}{4\Delta_k^2+\gamma_2^2}\hat{\sigma}_k^{ss}, \end{aligned}$$

$$\hat{H}_{\rm int}'(t) = -\sum_k\frac{2g\Delta_k\Omega_k e^{i(\bar{\Delta}'-\Delta_k)t}}{4\Delta_k^2+\gamma_2^2}\hat{a}\hat{\sigma}_k^{sg} + {\rm H.c.}$$

and

$$\begin{aligned}\hat{\mathcal{L}}_{k,gs}^{\rm eff}(t) &= \sqrt{\frac{\gamma_2}{2}}\left(\frac{\Omega_k}{2\tilde{\Delta}_k}\hat{\sigma}_k^{gs} + \frac{ge^{i(\bar{\Delta}'-\Delta_k)t}}{\tilde{\Delta}_k}\hat{a}\hat{\sigma}_k^{gg}\right), \\ \hat{\mathcal{L}}_{k,sg}^{\rm eff}(t) &= \sqrt{\frac{\gamma_2}{2}}\left(\frac{\Omega_k}{2\tilde{\Delta}_k}\hat{\sigma}_k^{ss} + \frac{ge^{i(\bar{\Delta}'-\Delta_k)t}}{\tilde{\Delta}_k}\hat{a}\hat{\sigma}_k^{sg}\right). \end{aligned}$$

Thus, we obtain the effective master equation (31) in the main text.

[1] A. André, L.-M. Duan, and M. D. Lukin, Coherent atom interactions mediated by dark-state polaritons, Phys. Rev. Lett. **88**, 243602 (2002).

[2] A. Sondberg Sørensen and K. Mølmer, Entangling atoms in bad cavities, Phys. Rev. A **66**, 022314 (2002).

[3] M. H. Schleier-Smith, I. D. Leroux, and V. Vuletić, Squeezing the collective spin of a dilute atomic ensemble by cavity feedback, Phys. Rev. A **81**, 021804(R) (2010).

[4] A. Chiocchetta, D. Kiese, C. P. Zelle, F. Piazza, and S. Diehl, Cavity-induced quantum spin liquids, Nat. Commun. **12**, 5901 (2021).

[5] A. W. Glaetzle, M. Dalmonte, R. Nath, C. Gross, I. Bloch, and P. Zoller, Designing frustrated quantum magnets with laser-dressed Rydberg atoms, Phys. Rev. Lett. **114**, 173002 (2015).

[6] M. A. Norcia, R. J. Lewis-Swan, J. R. K. Cline, B. Zhu, A. M. Rey, and J. K. Thompson, Cavity-mediated collective

spin-exchange interactions in a strontium superradiant laser, Science **361**, 259 (2018).

[7] J. Hu, W. Chen, Z. Vendeiro, A. Urvoy, B. Braverman, and V. Vuletić, Vacuum spin squeezing, Phys. Rev. A **96**, 050301(R) (2017).

[8] R. J. Lewis-Swan, M. A. Norcia, J. R. K. Cline, J. K. Thompson, and A. M. Rey, Robust spin squeezing via photon-mediated interactions on an optical clock transition, Phys. Rev. Lett. **121**, 070403 (2018).

[9] M. Morgado and S. Whitlock, Quantum simulation and computing with Rydberg-interacting qubits, AVS Quantum Sci. **3**, 023501 (2021).

[10] H. Levine, A. Keesling, G. Semeghini, A. Omran, T. T. Wang, S. Ebadi, H. Bernien, M. Greiner, V. Vuletić, H. Pichler, and M. D. Lukin, Parallel implementation of high-fidelity multiqubit gates with neutral atoms, Phys. Rev. Lett. **123**, 170503 (2019).

[11] C. J. Picken, R. Legaie, K. McDonnell, and J. D. Pritchard, Entanglement of neutral-atom qubits with long ground-Rydberg coherence times, Quantum Sci. Technol. **4**, 015011 (2018).

[12] Y.-Y. Jau, A. M. Hankin, T. Keating, I. H. Deutsch, and G. W. Biedermann, Entangling atomic spins with a Rydberg-dressed spin-flip blockade, Nat. Phys. **12**, 71 (2016).

[13] T. M. Graham, M. Kwon, B. Grinkemeyer, Z. Marra, X. Jiang, M. T. Lichtman, Y. Sun, M. Ebert, and M. Saffman, Rydberg-mediated entanglement in a two-dimensional neutral atom qubit array, Phys. Rev. Lett. **123**, 230501 (2019).

[14] S. J. Masson, M. D. Barrett, and S. Parkins, Cavity QED engineering of spin dynamics and squeezing in a spinor gas, Phys. Rev. Lett. **119**, 213601 (2017).

[15] C. Klempt, O. Topic, G. Gebreyesus, M. Scherer, T. Henninger, P. Hyllus, W. Ertmer, L. Santos, and J. J. Arlt, Parametric amplification of vacuum fluctuations in a spinor condensate, Phys. Rev. Lett. **104**, 195303 (2010).

[16] X.-Y. Luo, Y.-Q. Zou, L.-N. Wu, Q. Liu, M.-F. Han, M. K. Tey, and L. You, Deterministic entanglement generation from driving through quantum phase transitions, Science **355**, 620 (2017).

[17] I. D. Leroux, M. H. Schleier-Smith, and V. Vuletić, Implementation of cavity squeezing of a collective atomic spin, Phys. Rev. Lett. **104**, 073602 (2010).

[18] O. Hosten, R. Krishnakumar, N. J. Engelsen, and M. A. Kasevich, Quantum phase magnification, Science **352**, 1552 (2016).

[19] T. Moriya, New mechanism of anisotropic superexchange interaction, Phys. Rev. Lett. **4**, 228 (1960).

[20] T. Moriya, Anisotropic superexchange interaction and weak ferromagnetism, Phys. Rev. **120**, 91 (1960).

[21] F. Hellman, A. Hoffmann, Y. Tserkovnyak, G. S. D. Beach, E. E. Fullerton, C. Leighton, A. H. MacDonald, D. C. Ralph, D. A. Arena, H. A. Dürr, P. Fischer, J. Grollier, J. P. Heremans, T. Jungwirth, A. V. Kimel, B. Koopmans, I. N. Krivorotov, S. J. May, A. K. Petford-Long, J. M. Rondinelli *et al.*, Interface-induced phenomena in magnetism, Rev. Mod. Phys. **89**, 025006 (2017).

[22] M. Haze, Y. Yoshida, and Y. Hasegawa, Experimental verification of the rotational type of chiral spin spiral structures by spin-polarized scanning tunneling microscopy, Sci. Rep. **7**, 13269 (2017).

[23] N. Nishad, A. Keselman, T. Lahaye, A. Browaeys, and S. Tsesses, Quantum simulation of generic spin-exchange models in Floquet-engineered Rydberg-atom arrays, Phys. Rev. A **108**, 053318 (2023).

[24] D.-W. Wang, C. Song, W. Feng, H. Cai, D. Xu, H. Deng, H. Li, D. Zheng, X. Zhu, H. Wang, S.-Y. Zhu, and M. O. Scully, Synthesis of antisymmetric spin exchange interaction and chiral spin clusters in superconducting circuits, Nat. Phys. **15**, 382 (2019).

[25] W. Liu, W. Feng, W. Ren, D.-W. Wang, and H. Wang, Synthesizing three-body interaction of spin chirality with superconducting qubits, Appl. Phys. Lett. **116**, 114001 (2020).

[26] S. Fujimoto, Hall effect of spin waves in frustrated magnets, Phys. Rev. Lett. **103**, 047203 (2009).

[27] M. Hirschberger, R. Chisnell, Y. S. Lee, and N. P. Ong, Thermal Hall effect of spin excitations in a kagome magnet, Phys. Rev. Lett. **115**, 106603 (2015).

[28] Y. Lu, X. Guo, V. Koval, and C. Jia, Topological thermal Hall effect driven by spin-chirality fluctuations in frustrated antiferromagnets, Phys. Rev. B **99**, 054409 (2019).

[29] N. Mohanta, E. Dagotto, and S. Okamoto, Topological Hall effect and emergent skyrmion crystal at manganite-iridate oxide interfaces, Phys. Rev. B **100**, 064429 (2019).

[30] X. G. Wen, F. Wilczek, and A. Zee, Chiral spin states and superconductivity, Phys. Rev. B **39**, 11413 (1989).

[31] S. F. Qi and J. Jing, Chiral current in Floquet cavity magnonics, Phys. Rev. A **106**, 033711 (2022).

[32] D. De Bernardis, Z.-P. Cian, I. Carusotto, M. Hafezi, and P. Rabl, Light-matter interactions in synthetic magnetic fields: Landau-photon polaritons, Phys. Rev. Lett. **126**, 103603 (2021).

[33] P. Roushan, C. Neill, A. Megrant, Y. Chen, R. Babbush, R. Barends, B. Campbell, Z. Chen, B. Chiaro, A. Dunsworth, A. Fowler, E. Jeffrey, J. Kelly, E. Lucero, J. Mutus, P. J. J. O'Malley, M. Neeley, C. Quintana, D. Sank, A. Vainsencher *et al.*, Chiral ground-state currents of interacting photons in a synthetic magnetic field, Nat. Phys. **13**, 146 (2017).

[34] X. X. Li, J. B. You, X. Q. Shao, and W. Li, Coherent ground-state transport of neutral atoms, Phys. Rev. A **105**, 032417 (2022).

[35] X. Wu, F. Yang, S. Yang, K. Mølmer, T. Pohl, M. K. Tey, and L. You, Manipulating synthetic gauge fluxes via multicolor dressing of Rydberg-atom arrays, Phys. Rev. Res. **4**, L032046 (2022).

[36] E. Kuznetsova, S. I. Mistakidis, S. T. Rittenhouse, S. F. Yelin, and H. R. Sadeghpour, Engineering chiral spin interactions with Rydberg atoms, arXiv:2309.08795.

[37] B. Peropadre, D. Zueco, F. Wulschner, F. Deppe, A. Marx, R. Gross, and J. J. García-Ripoll, Tunable coupling engineering between superconducting resonators: From sidebands to effective gauge fields, Phys. Rev. B **87**, 134504 (2013).

[38] R. Asensio-Perea, A. Parra-Rodriguez, G. Kirchmair, E. Solano, and E. Rico, Chiral states and nonreciprocal phases in a Josephson junction ring, Phys. Rev. B **103**, 224525 (2021).

[39] Y. Maleki, C. Zhou, and M. S. Zubairy, Time-reversal-symmetry breaking in a scalable cavity QED lattice, Phys. Rev. A **108**, 063709 (2023).

[40] P. Kiefer, F. Hakelberg, M. Wittemer, A. Bermúdez, D. Porras, U. Warring, and T. Schaetz, Floquet-engineered vibrational dynamics in a two-dimensional array of trapped ions, Phys. Rev. Lett. **123**, 213605 (2019).

[41] Y. Taguchi, Y. Oohara, H. Yoshizawa, N. Nagaosa, and Y. Tokura, Spin chirality, Berry phase, and anomalous Hall effect in a frustrated ferromagnet, Science **291**, 2573 (2001).
[42] B. Bauer, L. Cincio, B. P. Keller, M. Dolfi, G. Vidal, S. Trebst, and A. W. W. Ludwig, Chiral spin liquid and emergent anyons in a kagome lattice Mott insulator, Nat. Commun. **5**, 5137 (2014).
[43] Y. Zhou, K. Kanoda, and T.-K. Ng, Quantum spin liquid states, Rev. Mod. Phys. **89**, 025003 (2017).
[44] F.-H. Wang, X.-L. Lu, J.-J. Zou, and Z.-L. Xiang, Chiral excitation flows of multinode network based on synthetic gauge fields, arXiv:2312.02009.
[45] Z. Tao, L. Zhang, X. Li, J. Niu, K. Luo, K. Yi, Y. Zhou, H. Jia, X. Zhang, S. Liu, T. Yan, Y. Chen, and D. Yu, Experimental realization of phase-controlled dynamics with hybrid digital–analog approach, npj Quantum Inf. **7**, 73 (2021).
[46] N. Nagaosa and Y. Tokura, Topological properties and dynamics of magnetic skyrmions, Nat. Nanotechnol. **8**, 899 (2013).
[47] Y. Tokunaga, X. Z. Yu, J. S. White, H. M. Rønnow, D. Morikawa, Y. Taguchi, and Y. Tokura, A new class of chiral materials hosting magnetic skyrmions beyond room temperature, Nat. Commun. **6**, 7638 (2015).
[48] N. Goldman and J. Dalibard, Periodically driven quantum systems: Effective Hamiltonians and engineered gauge fields, Phys. Rev. X **4**, 031027 (2014).
[49] J. H. Shirley, Solution of the Schrödinger equation with a Hamiltonian periodic in time, Phys. Rev. **138**, B979 (1965).
[50] N. Lambert, M. Cirio, M. Delbecq, G. Allison, M. Marx, S. Tarucha, and F. Nori, Amplified and tunable transverse and longitudinal spin-photon coupling in hybrid circuit-QED, Phys. Rev. B **97**, 125429 (2018).
[51] M. Reitz and C. Genes, Floquet engineering of molecular dynamics via infrared coupling, J. Chem. Phys. **153**, 234305 (2020).
[52] W. Zhang, R. Wu, C. Sun, C. Wu, and G. Wang, Entangling two Dicke states in a periodic modulated quantum system, Phys. Rev. A **109**, 013712 (2024).
[53] V. Novičenko, G. Žlabys, and E. Anisimovas, Flow-equation approach to quantum systems driven by an amplitude-modulated time-periodic force, Phys. Rev. A **105**, 012203 (2022).
[54] M. P. Silveri, J. A. Tuorila, E. V. Thuneberg, and G. S. Paraoanu, Quantum systems under frequency modulation, Rep. Prog. Phys. **80**, 056002 (2017).
[55] Y. Zhang, Y.-M. Liu, H. Yang, G.-C. Wang, T.-T. Hu, C.-F. Sun, and T.-Y. Zheng, Phase control of stationary light pulses due to a weak microwave coupling, Opt. Commun. **343**, 183 (2015).
[56] K. Seetharam, A. Lerose, R. Fazio, and J. Marino, Correlation engineering via nonlocal dissipation, Phys. Rev. Res. **4**, 013089 (2022).
[57] E. J. Davis, A. Periwal, E. S. Cooper, G. Bentsen, S. J. Evered, K. Van Kirk, and M. H. Schleier-Smith, Protecting spin coherence in a tunable Heisenberg model, Phys. Rev. Lett. **125**, 060402 (2020).
[58] E. J. Davis, G. Bentsen, L. Homeier, T. Li, and M. H. Schleier-Smith, Photon-mediated spin-exchange dynamics of spin-1 atoms, Phys. Rev. Lett. **122**, 010405 (2019).
[59] G. S. Agarwal and W. Harshawardhan, Realization of trapping in a two-level system with frequency-modulated fields, Phys. Rev. A **50**, R4465 (1994).
[60] G. S. Agarwal, Control of decoherence and relaxation by frequency modulation of a heat bath, Phys. Rev. A **61**, 013809 (1999).
[61] M. W. Noel, W. M. Griffith, and T. F. Gallagher, Frequency-modulated excitation of a two-level atom, Phys. Rev. A **58**, 2265 (1998).
[62] W. Harshawardhan and G. S. Agarwal, Multiple Landau-Zener crossings and quantum interference in atoms driven by phase modulated fields, Phys. Rev. A **55**, 2165 (1997).
[63] Y.-H. Chen, A. Miranowicz, X. Chen, Y. Xia, and F. Nori, Enhanced-fidelity ultrafast geometric quantum computation using strong classical drives, Phys. Rev. Appl. **18**, 064059 (2022).
[64] R. Li, D. Yu, S.-L. Su, and J. Qian, Periodically driven facilitated high-efficiency dissipative entanglement with Rydberg atoms, Phys. Rev. A **101**, 042328 (2020).
[65] C.-L. Hung, A. González-Tudela, J. I. Cirac, and H. J. Kimble, Quantum spin dynamics with pairwise-tunable, long-range interactions, Proc. Natl. Acad. Sci. USA **113**, E4946 (2016).
[66] E. Brion, L. H. Pedersen, and K. Mølmer, Adiabatic elimination in a lambda system, J. Phys. A: Math. Theor. **40**, 1033 (2007).
[67] C. Gonzalez-Ballestero, Tutorial: Projector approach to open quantum systems, arXiv:2305.19704.
[68] M. Chen, J. Tang, L. Tang, H. Wu, and K. Xia, Photon blockade and single-photon generation with multiple quantum emitters, Phys. Rev. Res. **4**, 033083 (2022).
[69] W. Shao, C. Wu, and X.-L. Feng, Generalized James' effective Hamiltonian method, Phys. Rev. A **95**, 032124 (2017).
[70] J. Choi, H. Zhou, H. S. Knowles, R. Landig, S. Choi, and M. D. Lukin, Robust dynamic Hamiltonian engineering of many-body spin systems, Phys. Rev. X **10**, 031002 (2020).
[71] S. Geier, N. Thaicharoen, C. Hainaut, T. Franz, A. Salzinger, A. Tebben, D. Grimshandl, G. Zürn, and M. Weidemüller, Floquet Hamiltonian engineering of an isolated many-body spin system, Science **374**, 1149 (2021).
[72] P. Scholl, H. J. Williams, G. Bornet, F. Wallner, D. Barredo, L. Henriet, A. Signoles, C. Hainaut, T. Franz, S. Geier, A. Tebben, A. Salzinger, G. Zürn, T. Lahaye, M. Weidemüller, and A. Browaeys, Microwave engineering of programmable XXZ Hamiltonians in arrays of Rydberg atoms, PRX Quantum **3**, 020303 (2022).
[73] W. Morong, K. S. Collins, A. De, E. Stavropoulos, T. You, and C. Monroe, Engineering dynamically decoupled quantum simulations with trapped ions, PRX Quantum **4**, 010334 (2023).
[74] P. Peng, X. Huang, C. Yin, L. Joseph, C. Ramanathan, and P. Cappellaro, Deep reinforcement learning for quantum Hamiltonian engineering, Phys. Rev. Appl. **18**, 024033 (2022).
[75] J.-N. Zhang, I. Arrazola, J. Casanova, L. Lamata, K. Kim, and E. Solano, Probabilistic eigensolver with a trapped-ion quantum processor, Phys. Rev. A **101**, 052333 (2020).
[76] W. Gong, Y. Kharkov, M. C. Tran, P. Bienias, and A. V. Gorshkov, Improved digital quantum simulation by non-unitary channels, arXiv:2307.13028.
[77] D. Layden, First-order Trotter error from a second-order perspective, Phys. Rev. Lett. **128**, 210501 (2022).
[78] H. Feshbach, Unified theory of nuclear reactions, Ann. Phys. (NY) **5**, 357 (1958).
[79] F. Reiter and A. S. Sørensen, Effective operator formalism for open quantum systems, Phys. Rev. A **85**, 032111 (2012).

[80] O. Kyriienko and A. S. Sørensen, Floquet quantum simulation with superconducting qubits, Phys. Rev. Appl. **9**, 064029 (2018).

[81] M. Sameti and M. J. Hartmann, Floquet engineering in superconducting circuits: From arbitrary spin-spin interactions to the Kitaev honeycomb model, Phys. Rev. A **99**, 012333 (2019).

[82] B. A. Moores, L. R. Sletten, J. J. Viennot, and K. W. Lehnert, Cavity quantum acoustic device in the multimode strong coupling regime, Phys. Rev. Lett. **120**, 227701 (2018).

[83] A. Stockklauser, P. Scarlino, J. V. Koski, S. Gasparinetti, C. K. Andersen, C. Reichl, W. Wegscheider, T. Ihn, K. Ensslin, and A. Wallraff, Strong coupling cavity QED with gate-defined double quantum dots enabled by a high impedance resonator, Phys. Rev. X **7**, 011030 (2017).

[84] Y. Liu, Z. Wang, P. Yang, Q. Wang, Q. Fan, S. Guan, G. Li, P. Zhang, and T. Zhang, Realization of strong coupling between deterministic single-atom arrays and a high-finesse miniature optical cavity, Phys. Rev. Lett. **130**, 173601 (2023).

[85] Y. Maleki, C. Zhou, and M. S. Zubairy, Time-reversal-symmetry breaking and chiral quantum state manipulation in plasmonic nanorings, Phys. Rev. A **105**, 042422 (2022).

[86] N. E. Palaiodimopoulos, S. Ohler, M. Fleischhauer, and D. Petrosyan, Chiral quantum router with Rydberg atoms, Phys. Rev. A **109**, 032622 (2024).

[87] Y. Maleki and A. M. Zheltikov, Witnessing quantum entanglement in ensembles of nitrogen-vacancy centers coupled to a superconducting resonator, Opt. Express **26**, 17849 (2018).

[88] N. Teper, Thermal preparation of an entangled steady state of distant nitrogen-vacancy-center ensembles, Eur. Phys. J. B **93**, 189 (2020).

[89] A.-H. Abdel-Aty, H. Kadry, A.-B. A. Mohamed, and H. Eleuch, Correlation dynamics of nitrogen vacancy centers located in crystal cavities, Sci. Rep. **10**, 16640 (2020).

[90] P. Neumann, N. Mizuochi, F. Rempp, P. Hemmer, H. Watanabe, S. Yamasaki, V. Jacques, T. Gaebel, F. Jelezko, and J. Wrachtrup, Multipartite entanglement among single spins in diamond, Science **320**, 1326 (2008).

[91] J. Harrison, M. Sellars, and N. Manson, Measurement of the optically induced spin polarisation of N-V centres in diamond, Diam. Relat. Mater. **15**, 586 (2006).

[92] A. Jarmola, V. M. Acosta, K. Jensen, S. Chemerisov, and D. Budker, Temperature- and magnetic-field-dependent longitudinal spin relaxation in nitrogen-vacancy ensembles in diamond, Phys. Rev. Lett. **108**, 197601 (2012).

[93] P. Z. Zhao, X. Wu, T. H. Xing, G. F. Xu, and D. M. Tong, Nonadiabatic holonomic quantum computation with Rydberg superatoms, Phys. Rev. A **98**, 032313 (2018).